Journal of Hazardous Materials 166 (2009) 103–108

Contents lists available at ScienceDirect

Journal of Hazardous Materials

journal homepage: www.elsevier.com/locate/jhazmat

Research Article

Fabrication and photocatalytic property of Pt-intercalated layered perovskite niobates $H_{1-x}LaNb_{2-x}Mo_xO_7$ ($x = 0$–0.15)

Yunfang Huang, Jing Li, Yuelin Wei, Yibin Li, Jianmin Lin, Jihuai Wu*

The Key Laboratory for College of Materials Science and Engineering, Huaqiao University of Fujian Higher Education, Institute of Materials Physical Chemistry, Huaqiao University, Quanzhou 362021, China

ARTICLE INFO

Article history:
Received 11 August 2008
Received in revised form 3 November 2008
Accepted 3 November 2008
Available online 21 November 2008

Keywords:
Semiconductors
Perovskite
$HLaNb_2O_7$
Photocatalytic properties

ABSTRACT

$H_{1-x}LaNb_{2-x}Mo_xO_7$ was prepared by solid-state reaction followed by an ion-exchange reaction. Pt was incorporated in the interlayer of $H_{1-x}LaNb_{2-x}Mo_xO_7$ by the stepwise intercalation reaction. The $H_{1-x}LaNb_{2-x}Mo_xO_7$ showed hydrogen production activity and the activities were greatly enhanced by Pt co-incorporating. The x value in $H_{1-x}LaNb_{2-x}Mo_xO_7$ had an important effect on the photocatalytic activity of the catalyst. When the $x = 0.05$, the $H_{1-x}LaNb_{2-x}Mo_xO_7$/Pt showed a photocatalytic activity of 80 $cm^3\ h^{-1}\ g^{-1}$ hydrogen evolution rate in 10 vol.% methanol solution under irradiation from a 100 W mercury lamp at 333 K.

1. Introduction

Hydrogen is considered as an ideal fuel for the future. However, presently, renewable energy contributes only about 5% of the commercial hydrogen production primarily via water electrolysis, while other 95% hydrogen is mainly derived from fossil fuels. Renewable hydrogen production is not popular yet because the cost is still high. Photovoltaic water electrolysis may become more competitive as the cost continues to decrease with the technology advancement. Photocatalytic water-splitting using semiconductor for hydrogen production offers a promising way for clean, low-cost and environmentally friendly production of hydrogen by solar energy [1–5]. In a recent review, a series of layered perovskite-related niobates, titanates, and titanoniobates has been prepared [6,7]. Their structures are very closely related to the Ruddlesden–Popper phase, and their general formulas are presented as $M[A_{n-1}B_nO_{3n+1}]$, where M is the interlayer cation, A is the cation surrounded by 12 oxygen atoms, and n describes the thickness of the perovskite slab. Representative catalysts reported so far include $K_2Ti_4O_9$ [8], $K_4Nb_6O_{17}$ [9], and $K_2La_2Ti_3O_{10}$ [10], which show potential activities for the decomposing of pure water. The relatively higher photocatalytic activity of these materials than that of the bulk-type simple oxides such as TiO_2 and ZnO has been ascribed to their peculiar structure such as layered or tunnel structures. One interesting feature of these complex mixed-oxides is that their catalytic activity can be highly improved by partial substitution on A- and/or B-sites, with only small changes in the average structure [11,12]. Another characteristic of these layered materials is that these photocatalysts use their interlayer space as reactions sites, where the electron–hole recombination process could be retarded by physical separation of the electron and hole pairs generated by photo-absorption. The interlayer guests are ion-exchangeable with various foreign species. The pillaring of layered compounds by inorganic compound is a promising method for fabricating function materials. Cationic species such as Ni^{2+} and Pt^{4+} have been introduced into interlayer galleries as precursors of photocatalytically active sites [13,14].

In our study, a new idea was released by replacing molybdenum atom with niobium atom in $HLaNb_2O_7$ lattice site and modifying with platinum. Since $HLaNb_2O_7$ is a perovskite and n-type semiconductor with high-photocatalytic activity [15], it is expected that the photocatalytic activity of $HLaNb_2O_7$ would be enhanced further.

2. Experimental

2.1. Chemicals

Mo-doped layered $HLaNb_2O_7$ (designated as $H_{1-x}LaNb_{2-x}Mo_xO_7$) was synthesized by the ion-exchange reaction of Mo-doped $KLaNb_2O_7$ (designated as $K_{1-x}LaNb_{2-x}Mo_xO_7$) in 1 mol dm^{-3} HCl at 333 K for 96 h with replacement of acid in each 24 h. $K_{1-x}LaNb_{2-x}Mo_xO_7$ were synthesized by calcining the mixture of K_2CO_3, Nb_2O_5, MoO_3 and La_2O_3 with the molar ratio of $1:2-x:2x:1$ at 1423 K in air for 24 h with one intermediate grinding after calcining for 12 h [16]. $[PtCl_6]^{2-}$ was incorporated in the inter-

* Corresponding author. Tel.: +86 595 22693899; fax: +86 595 22693999.
E-mail address: jhwu@hqu.edu.cn (J. Wu).

0304-3894/$ – see front matter © 2008 Published by Elsevier B.V.
doi:10.1016/j.jhazmat.2008.11.040

layer of $H_{1-x}LaNb_{2-x}Mo_xO_7$ by stirring $H_{1-x}LaNb_{2-x}Mo_xO_7$ (3 g) in 0.6 mmol dm^{-3} $(NH_4)_2PtCl_6$ aqueous solution (500 cm^3) at room temperature for 72 h, followed by UV light irradiation from a 400 W high-pressure mercury lamp at room temperature for 6 h to deposit Pt particles in its interlayer. Then the products were washed and dried at 283 K. The sample obtained was designated as $H_{1-x}LaNb_{2-x}Mo_xO_7$/Pt.

2.2. Analysis

The crystalline phases of the products were identified by X-ray diffraction (Bruker D8 ADVANCE) using graphite monochromatized Cu Kα (λ = 0.154 nm) radiation. The XRD data for indexing and cell-parameter calculation were collected in a scan mode with a scanning speed of 2°/min in the 2θ range between 2° and 60°. The band gap energies of the products were determined from the onset of diffuse reflectance spectra of the powders measured by using a Shimadzu Model UV-3100 ultraviolet–visible spectrophotometer. The specific surface areas of samples were measured by nitrogen gas adsorption (Quantachrome NOVA 4200 Model). The element contents were determined by atomic emission spectroscopy (Intretid xsp radil ict-aes).

2.3. Photochemical reaction

Photochemical reaction was carried out in a Pyrex reactor with a capacity of 500 cm^3, attached to an inner radiation-type 100 W high-pressure mercury lamp. The inner cell had thermostated water flowing through a jacket between the mercury lamp and reaction chamber and it was constructed of Pyrex glass, which cut the UV emission of the mercury below 290 nm. The photocatalytic activities of the catalyst were determined by measuring the amount of hydrogen gas evolved with a gas burette when the dispersed catalysts were irradiated. Prior to the reaction, the mixture was deaerated by evacuation and then flushed with N_2 (20 kPa) repeatedly to remove O_2 and CO_2 dissolving in water. Before irradiation, it was confirmed that no reaction occurred in the dark. The evolved gas was analyzed by gas chromatography (Shanghai, 102G, molecular sieve 5A column and Ar carrier).

3. Results and discussion

Fig. 1(a) shows the crystal structures for $KLaNb_2O_7$. The structure of the $KLaNb_2O_7$ compound can be described as double layered perovskite type structure made up of NbO_6 sheets with La ions filling in the interstice of the octahedron of NbO_6 and the K^+ ion in the interlayer [17]. The crystal structure of $KLaNb_2O_7$ has orthorhombic symmetry of space group $C222$ (a = 3.9060 nm, b = 21.6030 nm, c = 3.8879, Z = 2). When K^+ ions were proton exchanged, $HLaNb_2O_7$ with a layered perovskite-type structure was obtained and its structure was shown in Fig. 1(b). The crystal structure of $HLaNb_2O_7$ has tetragonal symmetry of space group $P4/m$ (a = 3.8886 nm, c = 10.5483, Z = 1). According to the X-ray diffraction date and calculation, the NbO_6 sheet is arranged in double layers and the height of the unit layer is 0.75 nm. The protons are arranged in the interlayer perpendicular to the c-axis, which allows a ready incorporation of guest molecules and the expansion of the c-parameter on intercalation.

Fig. 2 depicts XRD patterns of $K_{1-x}LaNb_{2-x}Mo_xO_7$ (x = 0–0.15). Some new peaks appeared when MoO_3 was doped in the system. This new peaks were probably attributed to $K_2LaNb_5O_{15}$ and $LaNbO_4$ according to the Joint Committee of Powder Diffraction Standard (JCPDS) data. With the increase of the amount of (x) MoO_3, the peak intensity of $KLaNb_2O_7$ decreased, whereas the peak intensity of $K_2LaNb_5O_{15}$ and $LaNbO_4$ all increased. Therefore, it is

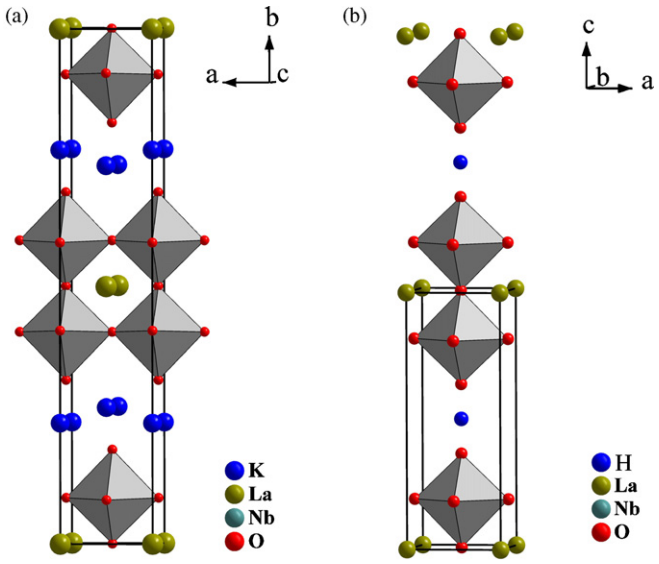

Fig. 1. Crystal structure of (a) $KLaNb_2O_7$ and (b) $HLaNb_2O_7$.

suspected that the following reaction might take place during the calcining:

$$2KLaNb_2O_7 + Nb_2O_5 \rightarrow K_2LaNb_5O_{15} + LaNbO_4 \quad (1)$$

It suggested that the appearance of $K_2LaNb_5O_{15}$ and $LaNbO_4$ were attributed to the replacement of Nb^{5+} by Mo^{6+}, the addition of Mo^{6+} induced the excess of Nb^{5+} and produced new phases. Similar phenomena were observed in Fig. 3. The new phases $K_2LaNb_5O_{15}$ and $LaNbO_4$ were also produced when excess amount of niobium oxide (25 mol%) was added in the stoichiometric mixture of K_2CO_3, La_2O_3 and Nb_2O_5 as the starting material. It is noticeable that no diffraction peaks corresponding to MoO_3 or containing Mo phase appeared. Ionic radii of 6-coordinated Mo^{6+} (0.62 nm) and Nb^{5+} (0.69 nm) ions are almost the same as each other, and the 6-coordinated Mo^{6+} ions substituted for Nb^{5+} ions in $KLaNb_2O_7$

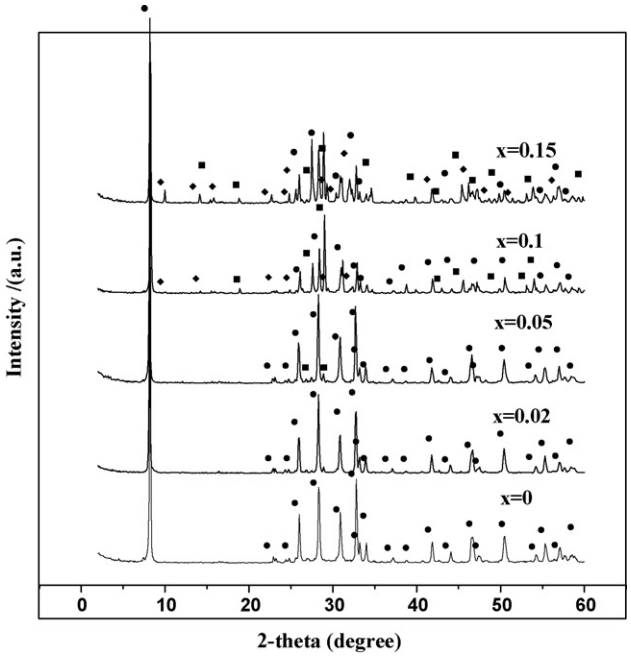

Fig. 2. X-ray powder diffraction patterns of the samples produced with the molar ratio for K_2CO_3, Nb_2O_5, MoO_3, La_2O_3 at 1:2 − x:2x:1 (●, $KLaNb_2O_7$; ■, $LaNbO_4$; ♦, $K_2LaNb_5O_{15}$).

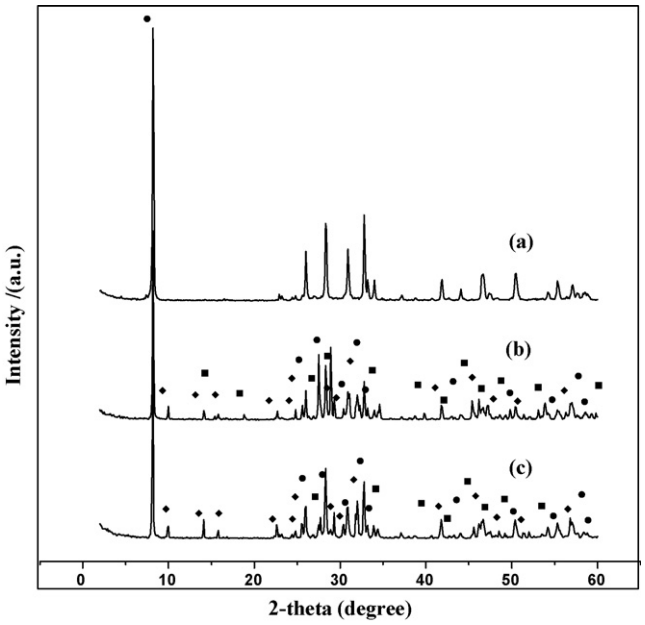

Fig. 3. X-ray powder diffraction patterns of: (a) $KLaNb_2O_7$, (b) $K_{1-x}LaNb_{2-x}Mo_xO_7$ ($x = 0.15$), (c) $KLaNb_2O_7$ (excess amount of niobium oxide 25 mol%): (●) $KLaNb_2O_7$; (■) $LaNbO_4$; (♦) $K_2LaNb_5O_{15}$.

crystal lattice site. In contrast, an ionic radius of the 12-coordinated La^{3+} ion (0.19 nm) is remarkably larger than that of the Mo^{6+} ion (0.69 nm). If La^{3+} ions which were at the position of A sites in perovskite structures were replaced with Mo^{3+} ions, a large shift should be observed. As MoO_3 content was increased ($x = 0$–0.15), the normal $KLaNb_2O_7$ crystal lattice was deflected, and thus the new compound $LaNbO_4$ and $K_2LaNb_5O_{15}$ were formed. As we know, when Nb^{5+} was replaced by Mo^{6+}, the extra electron slightly bound by molybdenum atom could serve as a donor and it could jump to the conduction band under visible light irradiation, thus resulting in the products absorption in the visible light region over 400 nm. In addition, because of the replacement of Nb^{5+} by Mo^{6+}, the number of alkaline metal cations held in the interlayer space decreased in order to maintain the charge balance between the layers and the interlayers, which caused the absence of hydration of the products [18].

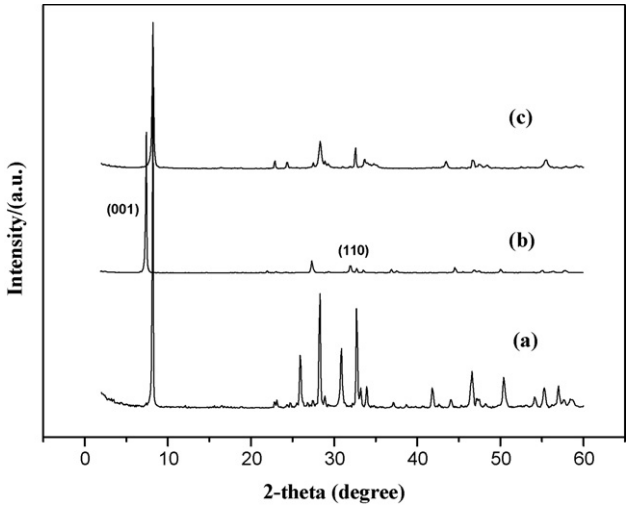

Fig. 4. X-ray powder diffraction patterns of: (a) $K_{1-x}LaNb_{2-x}Mo_xO_7$ ($x = 0.05$), (b) $H_{1-x}LaNb_{2-x}Mo_xO_7$ ($x = 0.05$), (c) $H_{1-x}LaNb_{2-x}Mo_xO_7$/Pt ($x = 0.05$).

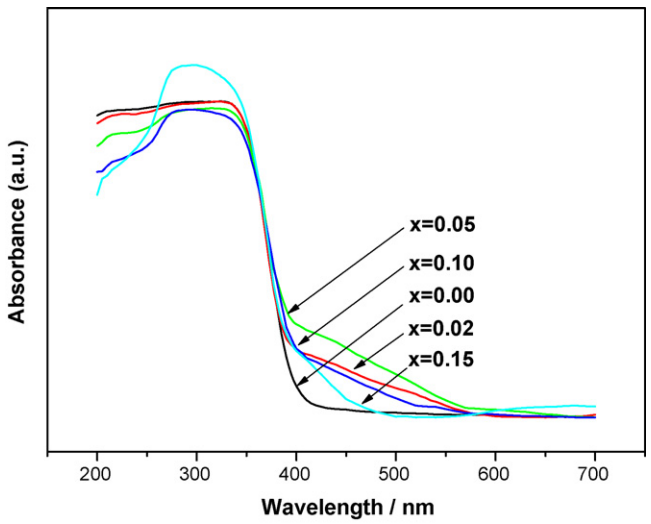

Fig. 5. Diffuse reflectance spectra of $H_{1-x}LaNb_{2-x}Mo_xO_7$ ($x = 0.0$, 0.02, 0.05, 0.10, 0.15).

Fig. 4 depicts the X-ray powder diffraction pattern of (a) $K_{1-x}LaNb_{2-x}Mo_xO_7$ ($x = 0.05$), (b) $H_{1-x}LaNb_{2-x}Mo_xO_7$ ($x = 0.05$), (c) $H_{1-x}LaNb_{2-x}Mo_xO_7$/Pt ($x = 0.05$). The powder X-ray diffraction patterns showed that protonated oxides $H_{1-x}LaNb_{2-x}Mo_xO_7$ retained the parent structure of $K_{1-x}LaNb_{2-x}Mo_xO_7$ except for a slightly decrease in the *c*-axis. Sample (c) showed no diffraction peak corresponding to Pt, indicating that Pt was incorporated in the interlayer. The diffraction peak positions corresponding to the (1 1 0) crystal face of samples (a), (b) and (c) were almost the same, but those corresponding to the (0 0 1) crystal face changed significantly depending on the species in the interlayer. The results suggested that layered structure of catalyst remained intact after intercalation of Pt, although the interlayer distances changed. When Pt was incorporated, the interlayer distance of $H_{1--x}LaNb_{2-x}Mo_xO_7$/Pt ($x = 0.05$) became 1.08 nm, and the pillar height of Pt determined by subtracting the $LaNb_{2-x}Mo_xO_7^-$ unit layer was 0.33 nm. A gallery height of Pt pillars of less than 0.5 nm indicated the formation of an intercalated nanomaterial, which was favored for the coupling of host and guest semiconductors and changed the enhancement of the photocatalytic activity.

Fig. 5 shows the UV–vis reflectance spectra of $H_{1-x}LaNb_{2-x}Mo_xO_7$. Compared with the white $KLaNb_2O_7$, both $H_{1-x}LaNb_{2-x}Mo_xO_7$ showed light purple to blue color with the increase of Mo-doping ratio from $x = 0.1$ to $x = 0.15$. When Mo was doped on $HLaNb_2O_7$, a new absorption was generated in the visible light region while the band gap absorption of $HLaNb_2O_7$ with absorption edge of 400 nm (3.10 eV) was not affected. The absorption edge of 560 nm was attributed to the charge transfer transition between the Mo ion d electrons and $HLaNb_2O_7$ conduction or valence band [19]. The energy gap of Mo-doped $HLaNb_2O_7$ was 2.2 eV, which suggested that the energy level of Mo^{6+} was at 2.2 eV more negative than the conduction band of $HLaNb_2O_7$. It is well known that light absorption by the material and the migration of the light-induced electrons and holes are the most key factors controlling a photocatalytic reaction, which is relevant to the electronic structure characteristics of the material. The process for photocatalysis of semiconductor is the direct absorption of photon by band gap of the materials and generates electron–hole pairs in the semiconductor particles [20]. The excitation of an electron from the valence band to the conduction band is initiated by light absorption with energy equal to or greater than the band gap of the semiconductor. Upon excitation, the photogenerated electron and hole can migrate to the surface of semiconductor. It is namely

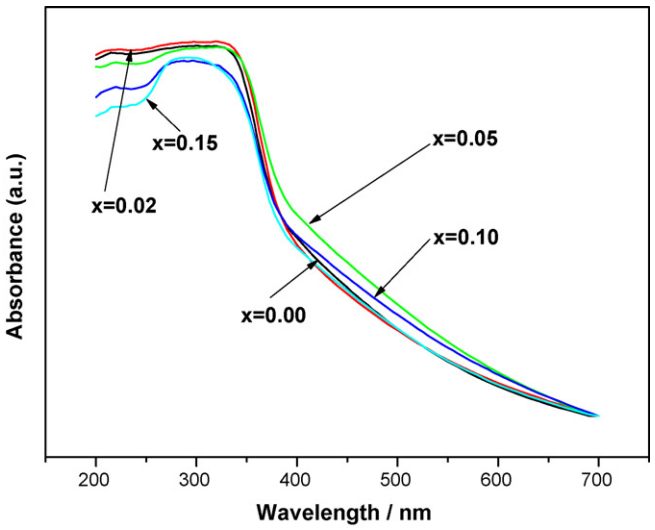

Fig. 6. Diffuse reflectance spectra of $H_{1-x}LaNb_{2-x}Mo_xO_7$/Pt (x = 0.0, 0.02, 0.05, 0.10, 0.15).

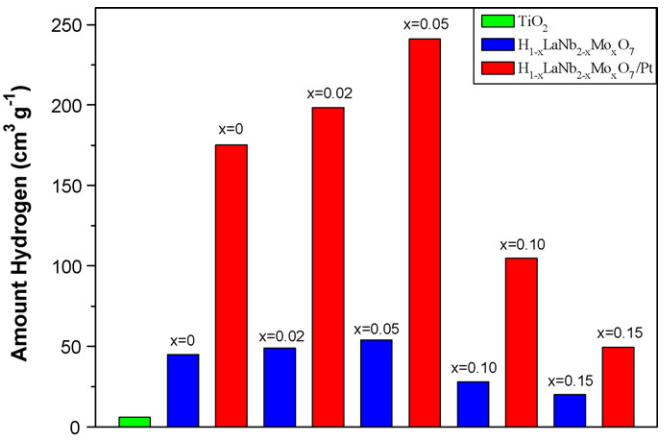

Fig. 7. Hydrogen production from 500 cm^3 of 10 vol.% methanol solution containing 1.0 g of dispersed samples exposed to irradiation from a 100 W mercury lamp at 333 K for 3 h.

that the narrower band gap of the semiconductor can harvest more photons to excite the electron from the valence band to the conduction band.

Fig. 6 shows the UV–vis reflectance spectra of $H_{1-x}LaNb_{2-x}Mo_xO_7$/Pt. Compared with $H_{1-x}LaNb_{2-x}Mo_xO_7$, $H_{1-x}LaNb_{2-x}Mo_xO_7$/Pt showed yellow color and a broad reflection spectra over 400–700 nm with two onsets corresponding to host $H_{1-x}LaNb_{2-x}Mo_xO_7$ and Pt. One can be attributed to $H_{1-x}LaNb_{2-x}Mo_xO_7$ which absorbs UV light, and the other was attributed to platinum which absorbs not only UV light but also visible light. The visible light absorption region might be due to the coupling effect of host and guest Pt and the quantum size effect of intercalated nanomaterial. Similar phenomena also were observed in $H_2Ti_4O_9$ and $H_4Nb_6O_{17}$ systems [21,22]. The amount of added platinum was that in a solution for ion-exchange procedure and not after aqua regia treatment. It was considered for those samples that a small amount of platinum remained on the external surface of catalyst. If the Pt content was too high, $H_{1-x}LaNb_{2-x}Mo_xO_7$ would be covered with the excess Pt on the surface (deposition of the metal on the photocatalyst). This could reduce the effective area of $H_{1-x}LaNb_{2-x}Mo_xO_7$ surface of for absorbance light. This would result in the decrease of absorbance for $H_{1-x}LaNb_{2-x}Mo_xO_7$ photocatalyst. Therefore, $H_{1-x}LaNb_{2-x}Mo_xO_7$/Pt (x = 0.05, Pt = 1.19 wt.%) showed the maximum visible light absorption.

The interlayer distance, content of Pt, band gap energy and specific surface area of the products were summarized in Table 1. The interlayer distance of $H_{1-x}LaNb_{2-x}Mo_xO_7$, in the range of 1.02–1.23 nm, seemed to decrease with increasing Mo-doping content, which might stem from the decrease in the hydrated capacity and the distorted structure caused by the Mo^{6+} replacement. On the other hand, after Pt was incorporated in the layer, the interlayer distance did not increase as expected until the Mo-doping content exceeded x = 0.1. It may be due to the absence of hydration in its layer as the samples were dried at 383 K. When the doping content was higher than x = 0.1, $H_{1-x}LaNb_{2-x}Mo_xO_7$ was hard to hydrate, thus the interlayer distance increased owing to the incorporation of Pt. The content of Pt appeared to increase with the increase of Mo-doping content, indicating that the increase in the interlayer distance was not necessarily helpful in increasing the amount of Pt incorporated. The specific surface area increased by doping molybdenum, which may be ascribed to the formation of such soluble phase as $KLaMoO_5$. As a result, some holes and pores were created when $KLaMoO_5$ was dissolved, which lead to the increasing of the specific surface area.

Fig. 7 shows the hydrogen gas evolution rates from 500 cm^3 of 0.1 mol dm^{-3} methanol solution containing 1 g of dispersed catalysts at 333 K under irradiation from a 100 W mercury lamp for 3 h. A significant amount of hydrogen was observed in the presence of host $H_{1-x}LaNb_{2-x}Mo_xO_7$ alone. The photocatalytic activity was increased with Mo content up to x = 0.05, but after this composition, it was decreased with Mo content. The highest activity was obtained over $H_{0.95}LaNb_{1.95}Mo_{0.05}O_7$ photocatalyst, the hydrogen produced amount was estimated to be 54 cm^3, which was larger than that of $HLaNb_2O_7$ (ca. 45 cm^3).

It is accepted that photocatalyst particles absorb light of energy greater than the band gap to generate electron/hole pairs (Eq. (1)) [23,24]. The electrons are photoinduced to the conduction band (e^-_{CB}) and the holes in the valence band (h^+_{VB}). In the absence of oxygen and presence of sacrificial species such as methanol, the holes generated by the light are trapped by H_2O to yield H^+ and •OH radicals (Eq. (2)), and subsequently the •OH radicals will oxidize methanol to HCHO, etc., while electrons in the conduction band of the particle will simultaneously reduce water or protons in the solution to form gaseous H_2 as shown by Eqs. (2)–(5). These reactions

Table 1
The interlayer distance, content of Pt, band gap energy and surface area of the samples.

Product	Interlayer distance (nm)	Content of Pt (wt.%)	Band gap energy (eV)	Specific surface area (m^2 g^{-1})
$HLaNb_2O_7$	1.23	0	3.1	4.18
$H_{1-x}LaNb_{2-x}Mo_xO_7$ (x = 0.02)	1.21	0	3.1	4.54
$H_{1-x}LaNb_{2-x}Mo_xO_7$ (x = 0.05)	1.20	0	3.1	11.50
$H_{1-x}LaNb_{2-x}Mo_xO_7$ (x = 0.15)	1.02	0	3.1	7.84
$HLaNb_2O_7$/Pt	1.05	1.34	3.1, 2.3	7.67
$H_{1-x}LaNb_{2-x}Mo_xO_7$/Pt (x = 0.02)	1.05	1.04	3.1, 2.3	7.50
$H_{1-x}LaNb_{2-x}Mo_xO_7$/Pt (x = 0.05)	1.08	1.19	3.1, 2.3	7.34
$H_{1-x}LaNb_{2-x}Mo_xO_7$/Pt (x = 0.15)	1.08	1.61	3.1, 2.3	9.76

proceed competitively with the recombination of the photoinduced electrons and holes.

On the basis of the above results, possible photoreactions on the photocatalysts were proposed as

$$Cat. \xrightarrow{h\nu} Cat.(h^+_{VB} + e^-_{CB}) \quad (1)$$

$$h^+_{VB} + H_2O \rightarrow \cdot OH + H^+ \quad (2)$$

$$CH_3OH + \cdot OH \rightarrow \cdot CH_2OH + H_2O \quad (3)$$

$$\cdot CH_2OH \rightarrow HCHO + H^+ + e^-_{CB} \quad (4)$$

$$2H_2O + 2e^-_{CB} \rightarrow H_2 + 2OH^- \quad (5)$$

The overall reaction is

$$CH_3OH \xrightarrow{h\nu} HCHO + H_2 \quad (6)$$

The optimum content of Mo doping at $x = 0.05$ may be due to the fact that there exists an optimum doping content of Mo ions in $HLaNb_2O_7$ particles for the most efficient separation of photoinduced electron–hole pairs. Pleskov [25] reported that the value of the space charge region potential for the efficient separation of electron–hole pairs must be no lower than 0.2 V. As the content of dopant ions increases, the surface barrier becomes higher, and the space charge region becomes narrower, the electron–hole pairs within the region are efficiently separated by the large electric field before recombination. On the other hand, when the content of doping is high, the space charge region becomes very narrow and penetration depth of light into catalyst greatly exceeds the space charge layer; therefore the recombination of the photogenerated electron–hole pairs in semiconductor become easier. There is an optimum content of dopant ions to make the thickness of space charge layer substantially equal to the light penetration depth. Secondly, a partial substitution of Nb^{5+} by Mo^{6+} leads to the decrease in the negative charge density of the perovskite interlayer and thus to the decrease of the number of H^+ cations located to maintain the charge balance at the interlayer space. So the water molecules are more easily intercalated into the interlayer space of $H_{1-x}LaNb_{2-x}Mo_xO_7$ which regard as a reaction site [26]. Consequently, the decrease of photocatalytic activity for higher Mo contents may be caused by the existence of an excess amount of rare earth oxide would increase the recombination centers and this increase will be detrimental to photocatalytic reactions [27]. Therefore, there exists an optimum Mo content that gives maximum photocatalytic activity.

The hydrogen gas evolution rate was greatly improved by constructing Pt for all samples. Pt has thus been demonstrated to be an excellent co-catalyst for H_2 production from water due to its low over-potential [13,20,28]. It is believed that the electric field at the $H_{1-x}LaNb_{2-x}Mo_xO_7$/Pt Schottky barrier diverts the photogenerated electrons to platinum leaving the holes in $H_{1-x}LaNb_{2-x}Mo_xO_7$. Efficient charge separation and electrocatalysis of H_2 evolution by platinum seems to be the cause of the high activity of $H_{1-x}LaNb_{2-x}Mo_xO_7$/Pt. As shown in Fig. 8, if the incident light energy is equal to or greater than the bandgap of the semiconductor, the electron (e^-) in the valance band can be excited to the conduction band. This energy change will result in the formation of positive holes (h^+) in valance band and free electrons in conduction band. However, the positive holes and electrons are easily recombined in a very short time, which will therefore lead to a very low activity of the photocatalyst. The deposited platinum in/on $H_{1-x}LaNb_{2-x}Mo_xO_7$ may play a very important role in preventing the rapid recombination between holes and electrons. Platinum can capture electrons generated from the surface of $H_{1-x}LaNb_{2-x}Mo_xO_7$, and thereby decrease the over-potential of H^+/H. The highest activity was obtained over $H_{0.95}LaNb_{1.95}Mo_{0.05}O_{10}$/Pt photocatalyst, the hydrogen produced amount was estimated to be 241 cm^3, which was 5.4 times larger than that of $HLaNb_2O_7$ (ca. 45 cm^3).

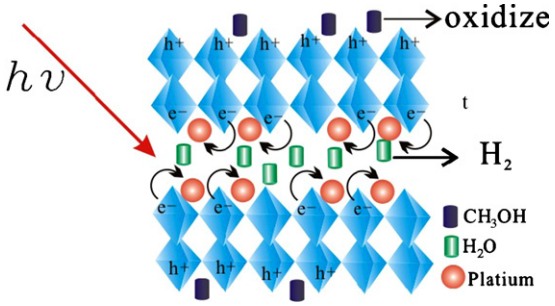

Fig. 8. Schematic structure of the $H_{1-x}LaNb_{2-x}Mo_xO_7$/Pt photocatalyst and the reaction mechanism of methanol solution decomposition into H_2.

4. Conclusions

In summary, a series of novel photocatalysts based on $n = 2$ members of Ruddlesden–Popper-type hydrous layered niobates with Mo doping was synthesized by solid-state method. Pt was incorporated into the interlayer of $H_{1-x}LaNb_{2-x}Mo_xO_7$ by successive reaction of $H_{1-x}LaNb_{2-x}Mo_xO_7$ with $(NH_4)_2PtCl_6$ aqueous solution. The photocatalytic activity of $H_{1-x}LaNb_{2-x}Mo_xO_7$ is increased with Mo content up to $x = 0.05$, but after this composition, it is decreased. $H_{1-x}LaNb_{2-x}Mo_xO_7$/Pt shows a broad reflection over 400–700 nm. The photocatalytic activity of $H_{1-x}LaNb_{2-x}Mo_xO_7$/Pt intercalated material is superior to TiO_2 (P25) and is enhanced by the co-incorporation of Pt. With use of $H_{0.95}LaNb_{1.95}Mo_{0.05}O_7$/Pt as a photocatalyst, the H_2 evolution is estimated to be 241 cm^3 for 3 h in the presence of methanol as a sacrificial agent under irradiation with $\lambda > 290$ nm for a 100 W mercury lamp. It is expected that the photocatalytic activity of $HLaNb_2O_7$ will be further improved by other modification in the next study.

Acknowledgements

The project was jointly supported by the National Natural Science Foundation of China (no. 50572030 and no. 50372022), the Key Scientific Technology Program of Fujian Province, China (no. 2005HZ01-4 and no. 2006J0439) and the Science Foundation of Huaqiao University (no. 08Q2R03 and no. 08BS408).

References

[1] A. Fujishima, K. Honda, Electrochemical photolysis of water at a semiconductor electrode, Nature 238 (1972) 37–38.
[2] M.R. Hoffmann, S.T. Martin, W. Choi, D.W. Bahnemann, Applications of semiconductor photocatalysis, Chem. Rev. 95 (1995) 69–96.
[3] R. Asahi, T. Morikawa, T. Ohwaki, K. Aoki, Y. Taga, Visible-light photocatalysis in nitrogen-doped titanium oxides, Science 293 (2001) 269–271.
[4] Z.G. Zou, J.H. Ye, K. Sayama, H. Arakawa, Direct splitting of water under visible light irradiation with an oxide semiconductor photocatalyst, Nature 414 (2001) 625–627.
[5] S.U.M. Khan, M. Al-Shah, W.B. Ingler, Efficient photochemical water splitting by a chemically modified n-TiO_2, Science 297 (2002) 2243–2245.
[6] H.W. Eng, P.W. Barnes, B.M. Auer, P.M. Woodward, Investigations of the electronic structure of d^0 transition metal oxides belonging to the pervoskite family, J. Solid State Chem. 175 (2003) 94–109.
[7] K. Tanabe, Catalytic application of niobium compounds, Catal. Today 78 (2003) 65–77.
[8] J.S. Wang, S. Yin, T. Sato, Characterization of $H_2Ti_4O_9$ with high specific surface area prepared by a delamination/reassembling process, Mater. Sci. Eng. B 126 (2006) 53–58.
[9] M.C. Sarahan, E.C. Carroll, M. Allen, D.S. Larsen, Ni.D. Browning, F.E. Osterloh, $K_4Nb_6O_{17}$-derived photocatalysts for hydrogen evolution from water: nanoscrolls versus nanosheets, J. Solid State Chem. 181 (2008) 1678–1683.
[10] C.T.K. Thaminimulla, T. Takata, M. Hara, J.N. Kondo, K. Domen, Effect of chromium addition for photocatalytic overall water splitting on Ni–$K_2La_2Ti_3O_{10}$, J. Catal. 196 (2000) 362–365.

[11] H. Xu, H.M. Li, C.D. Wu, J.Y. Chu, Y.S. Yan, H.M. Shu, Z. Gu, Preparation, characterization and photocatalytic properties of Cu-loaded $BiVO_4$, J. Hazard. Mater. 153 (2008) 877–884.
[12] G.K. Zhang, J. Zhou, X.M. Ding, Y.J. Hu, J.W. Xie, Characterization and photocatalytic properties of Ni-doped $Sr_{10}Bi_6O_{24-y}$, J. Hazard. Mater. (2008), doi:10.1016/j.jhazmat.2008.01.110.
[13] T. Chen, Z.C. Feng, G.P. Wu, J.Y. Shi, G.J. Ma, P.L. Ying, C. Li, Mechanistic studies of photocatalytic reaction of methanol for hydrogen on Pt/TiO_2 by in situ Fourier Transform IR and Time-Resolved IR spectroscopy, J. Phys. Chem. C 111 (2007) 8005–8014.
[14] H.Y. Lin, Y.F. Chen, Y.W. Chen, Water splitting reaction on $NiO/InVO_4$ under visible light irradiation, Int. J. Hydrogen Energy 32 (2007) 86–92.
[15] T. Matsuda, M. Udagawa, I. Kunou, Modification of the interlayer in lanthanunniobium oxide and its catalytic reactions, J. Catal. 168 (1997) 26–34.
[16] J. Gopalakrishnan, V. Bhat, $AlLaNb_2O_7$: a new series of layered perovskites exhibiting ion exchange and intercalation behaviour, Mater. Res. Bull. 22 (1987) 413–417.
[17] M. Sato, J. Abo, T. Jin, M. Ohta, Structure and ionic conductivity of $MlaNb_2O_7$ (M≡K, Na, Li, H), J. Alloys Compd. 192 (1993) 81–83.
[18] T. Takata, A. Tanaka, M. Hara, Recent progress of photocatalysts for overall water splitting, Catal. Today 44 (1998) 17–26.
[19] B. Enrico, J. Kiwi, M. Graetzel, E. Pelizzetti, M. Visca, Visible light induced water cleavage in colloidal solutions of chromium-doped titanium dioxide particles, J. Am. Chem. Soc. 104 (1982) 2996–3002.
[20] A.L. Linsebigler, G.Q. Lu, J.T. Yates, Environmental applications of semiconductor photocatalysis, Chem. Rev. 95 (1995) 735–758.
[21] S. Uchida, Y. Yamamoto, Y. Fujishiro, A. Watanabe, O. Ito, T. Sato, Intercalation of titanium oxide in layered $H_2Ti_4O_9$and $H_4Nb_6O_{17}$ and photocatalytic water cleavage with $H_2Ti_4O_9/(TiO_2$, Pt) and $H_4Nb_6O_{17}/(TiO_2$, Pt) nanocomposites, J. Chem. Soc. Faraday Trans. 93 (1997) 3229–3243.
[22] S. Tawkaew, S. Yin, T. Sato, Photoreduction of nitrate ion and photoevolution of hydrogen on unsupported TiO_2 and TiO_2 pillared $H_4Nb_6O_{17}$ nanocomposites, Int. J. Inorg. Mater. 3 (2001) 855–859.
[23] T. Kawai, T. Sakata, Photocatalytic hydrogen production from liquid methanol and water, J. Chem. Soc. Chem. Commun. 15 (1980) 694–695.
[24] H. Gerischer, A. Heller, The role of oxygen in photooxidation of organic molecules on semiconductor particles, J. Phys. Chem. 95 (1991) 5261–5267.
[25] Y.V. Pleskov, Conversion of luminous energy into electrical and chemical energy in photoelectrochemical cells with semiconductor electrodes (review), Sov. Electrochem. 17 (1981) 1–25.
[26] T. Takata, Y. Furumi, K. Shinohara, A. Tanaka, M. Hara, J.N. Kondo, K. Domen, Photocatalytic decomposition of water on spontaneously hydrated layered perovskites, Chem. Mater. (Commun.) 9 (1997) 1063–1064.
[27] J. Zhou, Y. Zhang, X.S. Zhao, A.K. Ray, Photodegradation of benzoic acid over metal-doped TiO_2, Ind. Eng. Chem. Res. 45 (2006) 3503–3511.
[28] T. Abe, E. Suzuki, M. Kaneko, Electron source in photoinduced hydrogen production on Pt-supported TiO_2 particles, J. Phys. Chem. B 103 (1999) 1119–1123.